Sounding the upper mesosphere using broadband solar occultation: The SOFIE experiment

Larry L. Gordley[a], Mark E. Hervig*[a], James M. Russell[b]
Chad Fish[c], Gregory J. Paxton[a], John C. Burton[a], Martin J. McHugh[a]
[a]GATS, Inc., 11864 Canon Blvd., Suite 101, Newport News, VA 23606
[b]Hampton University, 23 Tyler St., Hampton, VA 23668
[c]Space Dynamics Laboratory, Utah State University, Logan, UT

ABSTRACT

The Solar Occultation For Ice Experiment (SOFIE) is scheduled for launch onboard the Aeronomy of Ice in the Mesosphere (AIM) satellite in March 2007. SOFIE is designed to measure polar mesospheric clouds (PMCs) and the environment in which they form. SOFIE will conduct solar occultation measurements in 16 spectral bands that are used to retrieve vertical profiles of temperature, O_3, H_2O, CO_2, CH_4, NO, and PMC extinction at 10 wavelengths. Thirty occultations are observed each day covering latitudes from 65° - 85°S and 65° - 85°N. The PMC measurements are simultaneous with temperature and gas measurements that are unaffected by PMC signal. This data set will be the first of its kind, and allow new advancements in the understanding of the upper mesosphere.

Keywords: Solar Occultation, SOFIE, AIM, Mesosphere, PMC.

1. INTRODUCTION

The Solar Occultation For Ice Experiment (SOFIE) is one of three science instruments onboard the Aeronomy of Ice in the Mesosphere (AIM) satellite. The AIM goal is to characterize polar mesospheric clouds (PMCs) and the environment in which they form. PMCs, also known as noctilucent clouds (NLCs), exist near 83 km altitude during polar summer and are visible with the naked eye. PMCs are observed to vary over latitude, between hemispheres, and on seasonal and decadal time scales. Even more intriguing is the mounting evidence for long-term increases in PMC activity. Composed of ice particles[1], PMCs respond to atmospheric temperature, humidity, and the presence of ice nuclei. The observed increase in PMC frequency and brightness towards the poles is well correlated with decreasing temperatures as the poles are approached. Many observations indicate that PMCs are brighter and more numerous in the northern hemisphere than in the south[2]. Hemispheric PMC differences are attributed primarily to colder temperatures in the north, since mesospheric humidity appears to be nearly identical in the north and south[3]. Decadal variability in PMCs has been correlated with the 11-year solar cycle[4], during which solar intensity at certain wavelengths can change by a factor of two. Because water vapor is destroyed by solar lyman alpha radiation and increased solar intensity enhances diabatic heating, a warmer and drier mesosphere at solar maximum should result in fewer and dimmer PMCs. These expected relationships were recently quantified using measurements from the Halogen Occultation Experiment (HALOE)[3]. Finally, long-term changes in PMC characteristics are expected to result from anthropogenic climate forcing[5]. Increasing atmospheric carbon dioxide and methane have been linked to decreasing temperatures and higher humidity in the mesosphere. Since these changes are qualitatively consistent with increased PMC activity, PMCs were proposed as a visible indicator of atmospheric change[5]. PMCs are occurring more often, becoming brighter, and are now being sighted at middle latitudes for the first time[6]. Documenting long-term PMC changes and substantiating the connections between PMCs and climate change and has been challenging due to limitations in the observations of PMCs and their environment. While compelling evidence for long-term change exists[7], open questions concerning the drivers behind PMC formation and variability have roused debate over the interpretation of these findings[8,9].

*m.e.hervig@gats-inc.com; phone 208-354-8887; gats-inc.com

Infrared Spaceborne Remote Sensing XIV, edited by Marija Strojnik, Proc. of SPIE
Vol. 6297, 62970G, (2006) · 0277-786X/06/$15 · doi: 10.1117/12.682050

Increased understanding of natural processes and variability in the mesosphere is essential to developing a clearer picture of PMC changes on a variety of scales. SOFIE measurements will add to this understanding by providing vertical profiles of temperature, gaseous abundance (O_3, H_2O, CO_2, CH_4, and NO), and PMC extinction at 10 wavelengths from 0.29 – 5.3 μm. The SOFIE measurement suite is conducted simultaneously, and the key measurements of temperature, H_2O, and PMCs are independent of each other. SOFIE thus presents the first global data set of simultaneous uncorrupted temperature, H_2O, and PMC measurements. The SOFIE instrument draws on heritage from the highly successful HALOE instrument[10] which conducted solar occultation measurements from October 1991 thru November 2005. While HALOE offered simultaneous temperature (T), H_2O, and PMC measurements, the T and H_2O retrievals were contaminated by PMC interference and required corrections to be applied.

1.1. Measurement Approach

SOFIE uses the technique of satellite solar occultation to measure vertical profiles of limb path atmospheric transmission within 16 spectral bands between 0.29 - 5.32 μm wavelength. Occultation measurements are accomplished by monitoring solar intensity as the satellite enters or exits the Earth's sunlit side (spacecraft sunrise or sunset, see Figure 1). The ratio of solar intensity measured through the atmosphere to the intensity measured outside the atmosphere (exoatmospheric) yields atmospheric transmissions, which are the basis for retrieving physical properties. Because the atmospheric and exoatmospheric intensities are measured using the same electro-optical system, a variety of instrumental errors are eliminated when calculating transmission. SOFIE conducts broadband differential absorption measurements using eight channels. Each channel consists of two broadband radiometers, one located in a wavelength region of strong absorption and one in an adjacent a region of weaker absorption (see Table 1). SOFIE measures the strong and weak radiometer signals (V_S and V_W) and the difference of these (ΔV) which is amplified by an electronic gain, $G_{\Delta V}$.

$$\Delta V = (V_w - V_s)\, G_{\Delta V} \tag{1}$$

The SOFIE radiometer measurements can be written as integrals in wavelength (λ) and elevation angle (ϕ)

$$V = C \int_{\phi} \int_{\lambda} S(\phi,\lambda)\Gamma(\lambda)F(\phi)\tau_A(\phi,\lambda,q,P,T)\,d\phi\,d\lambda \tag{2}$$

where C is the instrument response constant, $S(\phi,\lambda)$ is the solar source function, $\Gamma(\lambda)$ is the instrument spectral response function, $F(\phi)$ is the field-of-view (FOV) response function, and $\tau_A(\phi,\lambda,q,P,T)$ is the atmospheric transmission for gas mixing ratio q at a given pressure (P) and temperature. The generally stratified nature of the upper atmosphere allows the effects of horizontal variability to be ignored.

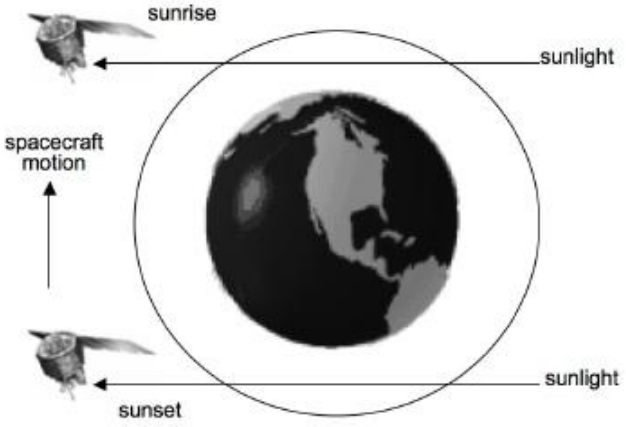

Fig. 1. Solar occultation measurement geometry depicting solar rays passing through the limb of the Earth's atmosphere during spacecraft sunrise and sunset.

Since the broadband atmospheric attenuation (A) is a function of the limb path optical depth (σ), $A = 1 - \exp(-\sigma)$, the measurement can be described by $V \approx S \exp(-\sigma)$. Above the atmosphere $\sigma = 0$ and $V = V_0 \approx S$ where V_0 is the exoatmospheric signal. Using the weak band measurement where $\sigma_W \approx 0$, and strong band mesurement where σ_S is non-zero but still very small, it can be shown show that

$$A = \frac{V_W - V_S}{V_0} \approx \frac{S - S\exp(-\sigma_S)}{S} = \sigma_S \tag{3}$$

Since $\Delta V/V_0$ is a ratio of measurements, absolute calibration of V_W and V_S are not critical. V_W and V_S are balanced exoatmospherically so that $V_W \approx V_S \approx V_0$. Thus, high precision measurements of the atmospheric attenuation A are accomplished thru high precision measurements of ΔV.

Difference signals allow extraordinarily precise isolation of the target gas signals. Once the gaseous signal has been isolated and the gas mixing ratio retrieved, the target gas signal can be calculated for any band and removed from the measured signal. At mesospheric altitudes, the remaining signal is due only to PMC extinction, especially in the weak bands. Thus, particle measurements can be made using each gas channels weak band (six wavelengths). SOFIE has two differential channels dedicated to PMC measurements (four wavelengths), so that PMCs will be measured at a total of 10 wavelengths. CO_2 measurements at 2.8 and 4.3 μm (channels 4 and 7) will be used to simultaneously retrieve CO_2 mixing ratio and temperature. While a single band measurement alone can be sufficient to retrieve gas mixing ratios in the lower mesosphere and stratosphere, SOFIE seeks to characterize the tenuous regions extending into the lower thermosphere. At these altitudes, atmospheric densities and gaseous abundances are low and the corresponding signals can approach the noise level. However, common mode errors are greatly reduced by measuring the difference in intensity between adjacent strong and weak absorption bands. Benefits are realized because a variety of atmospheric and instrumental effects are nearly identical in the strong and weak bands, and are therefore removed by differencing band pairs. For example, contaminant PMC absorption is nearly identical in the strong and weak bands, and therefore is removed in the difference signal measurements. Another benefit is that electronic gain can be applied to the difference signals, allowing the measurement precision to be enhanced to a level consistent with the system noise.

Table 1. SOFIE Channel Characteristics.

Channel	Band	Target (s = strong, w = weak)	Center Wavelength (μm)	Detector	Difference Signal gain, $G_{\Delta V}$
1	1	O_3 s	0.291	PV, SiC	30
	2	O_3 w	0.330	PV, SiC	
2	3	PMC s	0.867	PV, Ge	300
	4	PMC w	1.04	PV, Ge	
3	5	H_2O w	2.46	PC, HgCdTe	96
	6	H_2O s	2.62	PC, HgCdTe	
4	7	CO_2 s	2.79	PC, HgCdTe	110
	8	CO_2 w	2.94	PC, HgCdTe	
5	9	PMC s	3.06	PC, HgCdTe	120
	10	PMC w	3.12	PC, HgCdTe	
6	11	CH_4 s	3.38	PC, HgCdTe	202
	12	CH_4 w	3.48	PC, HgCdTe	
7	13	CO_2 s	4.32	PC, HgCdTe	110
	14	CO_2 w	4.65	PC, HgCdTe	
8	15	NO w	5.01	PC, HgCdTe	300
	16	NO s	5.32	PC, HgCdTe	

1.2. Measurement Geometry

The AIM satellite will be in a 600 km circular polar orbit. In this orbit, SOFIE provides sunset measurements at latitudes between about 65° and 85°S and sunrise measurements at latitudes between about 65° and 85°N (Figure 2). SOFIE observes 15 sunrise and 15 sunset occultations each day, and consecutive sunrise or sunset occultations are separated by 96 minutes or 24° longitude. In the AIM orbit, the Earth-relative solar sink rate is ~2.5 km s^{-1}. The SOFIE measurement suite consisting of 16 radiometer and 8 difference signal measurements is accomplished at 20 Hz, which corresponds to a vertical distance of 150 m in the atmosphere. Because the vertical resolution is about 1.5 km, the natural frequency of the data set is about 2 Hz, which is the rate at which the FOV dimension is swept through the atmosphere. SOFIE views the sun head-on and the atmosphere is sampled from 0 to 150 km in about 60 seconds.

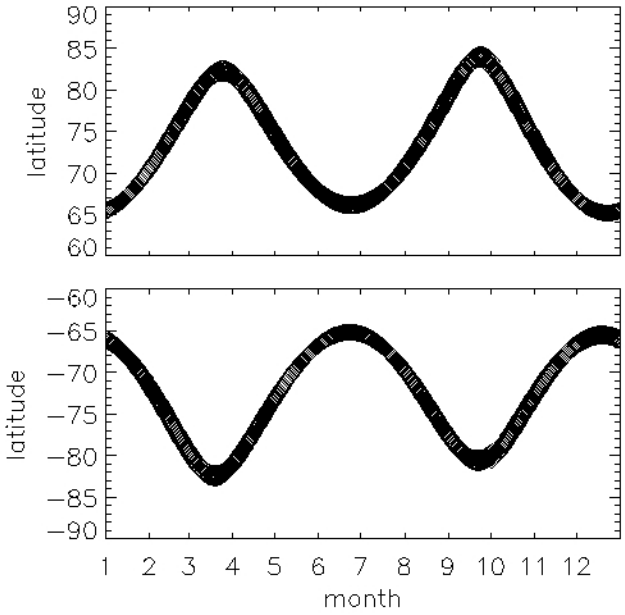

Figure 2. Predicted SOFIE measurement coverage for the first year on orbit. Sunrise measurements are at northern latitudes and sunset measurements are in the south.

2. INSTRUMENT DESCRIPTION

Principal components of the SOFIE instrument include the main telescope, sun sensor, and channel separation module (CSM). The SOFIE electronics are housed in a separate box that is located within the AIM spacecraft.

2.1. Optics

SOFIE uses a cassegrain telescope with a 10.16 cm entrance pupil. An elliptical steering mirror (16.76 × 11.55 cm) directs the incoming beam onto a focusing mirror and then to a secondary mirror (see Figure 3). The backside of the secondary mirror contains a pickoff mirror that directs a portion of the beam into the sun sensor module. The main beam passes through a field stop that determines the instantaneous field of view (IFOV). The field stop is 1.95 vertical × 4.74 arcmin horizontal, which is 1.50 × 3.63 km when projected to the 83 km limb path tangent point. The beam is chopped at 1000 Hz using a tuning fork device, and directed into the CSM where the science measurements are accomplished.

Within the CSM, energy is divided into 16 spectral bands using a combination of dichroic beam splitters and bandpass filters (see Figure 3). The CSM consists of four modules, each containing four bands that are close in wavelength. Spectral division within each CSM module is accomplished using cascading filters, which accept energy within the desired bandpass and reflect all other wavelengths. After the bandpass filter, the beam encounters a parabolic mirror

which directs it onto the detector. All detectors are mounted on three-stage thermo-electric coolers and packaged within a vented housing that contains an anti-reflective window. Bands 1 and 2 use 1 mm square photo-voltaic silicon carbide (SiC) detectors and bands 3 and 4 use 1 mm diameter photo-voltaic germanium (Ge) detectors. The infrared (IR) detectors (bands 5-16) are 1 mm square photo-conductive HgCdTe (MCT) devices (Table 1).

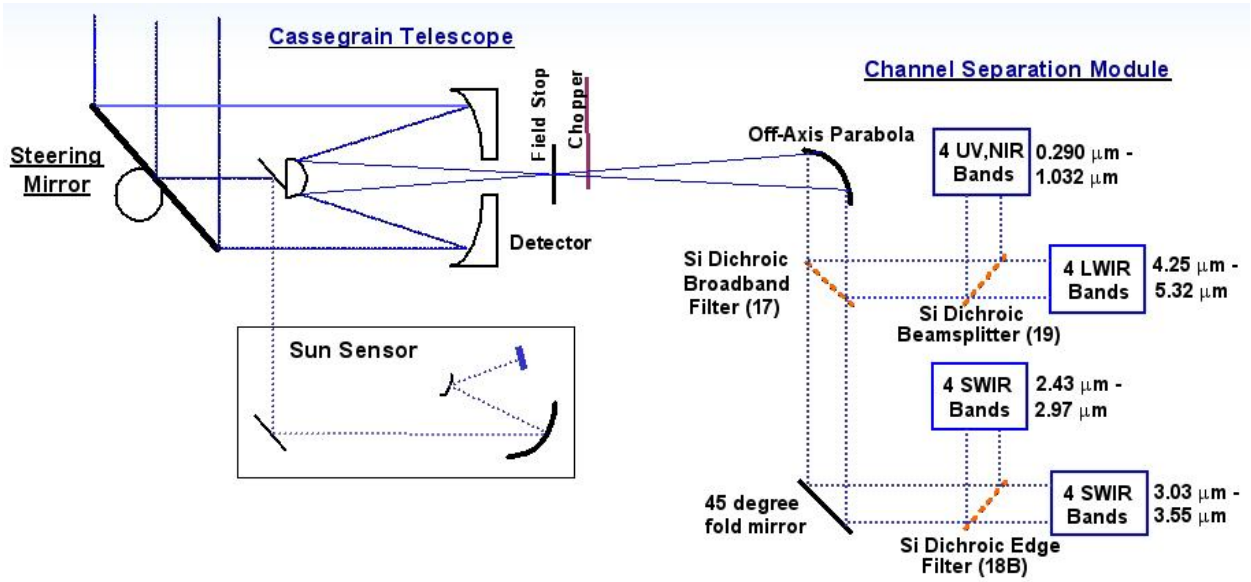

Figure 3. SOFIE optical system block diagram.

The sun sensor intercepts a portion of the incoming solar beam immediately after the steering mirror (Figure 3). This beam is directed through a neutral density filter to reduce intensity and a bandpass filter which designates the wavelength of 701.4 ± 11.5 nm. The sun is imaged using a radiation hardened focal plane array (FPA) comprised of 1024 x1024 pixels. The FPA field of view is 2.04° in azimuth and 2.025° in elevation (roughly 83 × 83 km at tangent). Individual FPA diodes are 15 μm square, and subtend roughly 7.14 arcsec at tangent. The apparent solar disc at tangent occupies ~32 arcmin (or 22 km), so that the sun sensor FPA can easily encompass the entire solar image. Incoming light is dispersed by the sun sensor optics according to an Airy disc function which determines a spot diameter of about 20 arcsec (FWHM). This blur actually increases the ability to determine the solar edge location. Analysis of the FPA data allows the position of the sun to be determined with ±1 arcsec uncertainty. The sun sensor determines the location of the top edge of the sun with respect to the science FOV. This information is used in determining the portion of the measured solar source function to use in (2) when simulating the SOFIE signals during measurement inversion.

2.2. Signal Conditioning Electronics

Three measurements are accomplished for each channel, the weak and strong band radiometer signals (V_w and V_s) and the difference of these signals (ΔV). A block diagram of the SOFIE analog signal path from detector to digitization is illustrated in Figure 4. Output signals from the detector preamp undergo signal conditioning including synchronous rectification at 1000 Hz. SOFIE signals are digitized using a 14 bit converter operating from -3 to 3 V. The signals are oversampled to determine statistical 16 bit values (91.6 μV / count) that are reported at 20 Hz. The radiometer signals operate between 0 and 2^{15} counts (0 to 3V) and thus provide a granularity in measured transmission of 3.052×10^{-5}. The ΔV measurements operate from -2^{15} to 2^{15} (-3 to 3V) counts and thus offer grannularity from 5.09×10^{-7} to 5.09×10^{-8} for $G_{\Delta V}$ from 30 to 300.

The weak and strong band signals have controllable attenuators that can induce gains (G_W and G_S, respectively) of 0 - 1 which are set through a 12 bit A/D controller. The ΔV signals are balanced to a deseried level, ΔV_{bal}, using the strong and/or weak band attenuators. For sunsets ΔV_{bal} is set while viewing the sun prior to encountering the atmosphere. G_W and G_S are set prior to sunrise to give the desired ΔV_{bal} setting that will occur exoatmospherically. At the end of a sunrise event ΔV is balanced exoatmospherically and the attenuator settings are used to predict the appropriate gain

settings for upcomming sunrise events. ΔV_{bal} can cover a range of values, with the greatest dynamic range realized for ΔV_{bal} = -3V. Because the atmosphere can induce small negative difference signals in a few cases, ΔV_{bal} is generally set slightly higher than -3V. The ΔV balance precision is a function of the attenuator step size (G_W and G_S) and the ΔV gain. The attenuators are 12 bit devices, and thus provide granularity of 1 part in 4096. The change in ΔV for a one count change in G_W or G_S is (2^{16} counts/ 6V) * ($3V/2^{12}$ counts) $G_{\Delta V}$ (in counts). The precision is half the step size, so the ΔV balance precision ranges from 120 to 1200 counts for $G_{\Delta V}$ from 30 to 300.

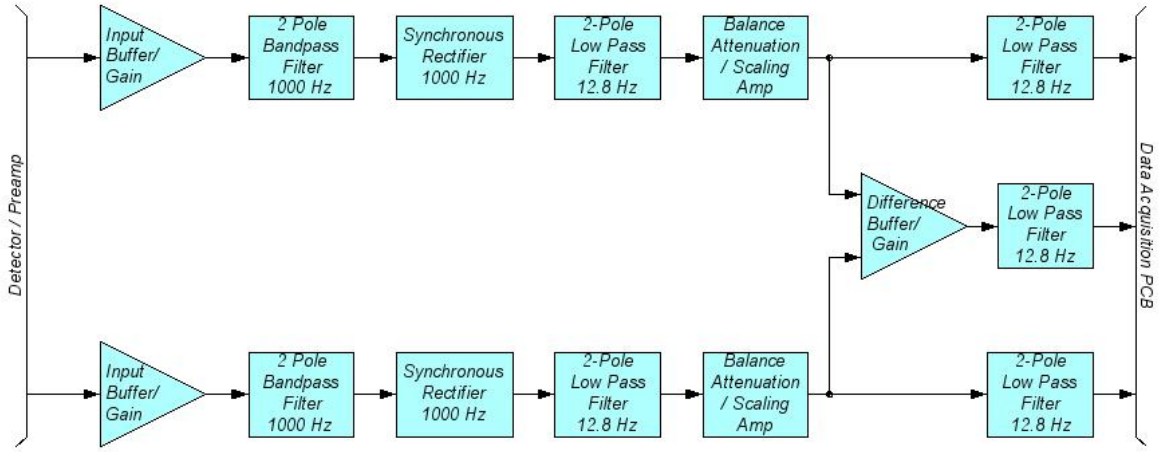

Figure 4. Electrical block diagram for a SOFIE band pair detector. The two paths represent the strong and weak band signal chains.

3. MEASUREMENT RETRIEVALS

Retrievals of geophysical quantities from SOFIE measurements rely on the ability to simulate the SOFIE measurements. The signal simulations must first describe radiative transfer of sunlight through the limb of the Earth's atmosphere, and then account for instrumental effects. Atmospheric transmissions are simulated using rigorous line-by-line radiative transfer calculations[11] with gaseous line parameters from the HITRAN 2000 data base. The radiative transfer model (LINEPAK) assumes a spherically symmetric atmosphere (onion peeling geometry). The simulated transmissions are convolved spatially over the SOFIE FOV response and spectrally over the measured solar source function. The simulated transmissions are then converted to counts based on the measured exoatmospheric signals and the instrument response function. For ΔV, the weak and strong band signals are modeled as above, and the simulated ΔV is determined using equation (1) with the known difference signal gain. The simulated signal is compared to the measurement, and the target gas mixing ratio, Q, is adjusted based on the derivative $\delta V/\delta Q$, which considers the previous attempt to match the measurement. Iteration continues at a given altitude until the measured signal is reproduced to within the noise.

Measurements of SOFIE performance during instrument calibration were used with model calculations to determine the expected retrieval performance. Signals were simulated using expected atmospheric conditions, and measured noise levels were applied to these signals. The simulated measurements were then used to retrieve atmospheric parameters, with retrieval performance determined by comparing the inversion results with the input atmospheric conditions. Example results for simulated H_2O retrievals are shown in Figure 5, indicating less than 10% uncertainties at altitudes below 100 km. Similar studies were conducted for all SOFIE retrievals and the results are summarized in Table 2.

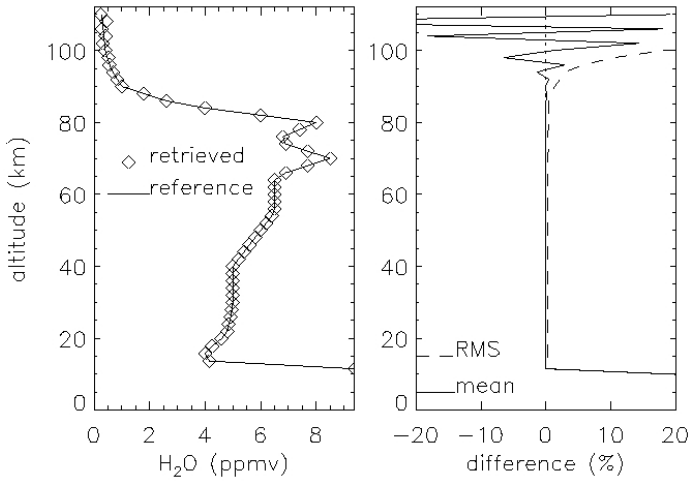

Figure 5. Results from simulated SOFIE water vapor retrievals. The left panel shows the average of 10 retrievals compared to the H_2O used to simulate the SOFIE measurements. The right panel shows average and RMS differences between the original and retrievedH_2O.

During an occultation event, solar rays are refracted by the Earth's atmosphere towards higher densities (towards Earth). Sun sensor measurements of vertical solar extent are used to determine the atmospheric refraction angle versus altitude. The altitude dependence of refraction angle is directly related to the atmospheric density profile. Assuming hydrostatic equilibrium, a measured refraction angle profile can therefore be used to retrieve the temperature profile with a high degree of accuracy and excellent vertical resolution. This basic approach was pioneered using Global Positioning Satellite data. The expected performance of the SOFIE refraction angle temperature retrieval was investigated by simulating the measured 705 nm refraction angle profile and using these results in a temperature retrieval. The results indicate that this approach will provide accurate temperatures from the surface to about 50 km altitude. Combining these retrievals with temperatures retrieved from the CO_2 transmission measurements will provide results extending from the surface to 100 km.

Table 2. Expected Performance of SOFIE Measurement Retrievals.

Retrieval	Precision Estimate at 83 km altitude	Altitude Range (km)
T	2.8 K	1 - 100
O_3	1 ppbv	15 – 100
H_2O	0.15 ppmv	15 – 100
CO_2	5.3 ppmv	15 – 100
CH_4	30 ppbv	15 – 95
NO	2×10^7 cm^{-3}	80 – 120
PMC	10^{-7} (V), 10^{-9} (ΔV)	Cloud

4. SUMMARY

The SOFIE instrument was completed during the spring of 2006 and assessments of instrument performance indicated that all systems were meeting or exceeding specification. SOFIE was delivered for integration on the AIM spacecraft, and the expected launch data is set for March 2007. The nominal AIM mission lifetime is 25 months, which will provide observations of two PMC seasons in each hemisphere. SOFIE will provide new information concerning PMCs and the environment in which they form, allowing significant advancement in our understanding of the upper mesosphere.

REFERENCES

1. Hervig, M. E., R. E. Thompson, M. McHugh, L. L. Gordley, J. M. Russell III, and M. E. Summers, First confirmation that water ice is the primary component of polar mesospheric clouds, *Geophys. Res. Letters, 28*, 971-974, 2001.
2. DeLand, M. T., E. P. Shettle, G. E. Thomas, and J. J. Olivero, Solar backscattered ultraviolet (SBUV) observations of polar mesospheric clouds (PMCs) over two solar cycles, *J. Geophys. Res., 108(D8)*, 8445, doi:10.1029/2002JD002398, 2003.
3. Hervig, M., and D. Siskind, Decadal and inter-hemispheric variability in polar mesospheric clouds, water vapor, and temperature, *J. Atmos. Solar-Terr. Phys.*, doi:10.1016/j.jastp.2005.08.010, 2005.
4. Gadsden, M., 1998. The North-West Europe data on noctilucent clouds: A survey. Journal of Atmospheric and Solar-Terrestrial Physics, 60, 1163-1174.
5. Thomas, G. E., Is the polar mesosphere the miner's canary of global change?. *Adv. Space Res., 18*, 149-158, 1996.
6. Wickwar, V. B., M. J. Taylor, J. P. Herron, and B. A. Martineau, Visual and lidar observations of noctilucent clouds above Logan, Utah, at 41.7°N, *J. Geophys. Res*., 10.1029/2001JD001180, 2002.
7. Shettle, E. P., Thomas, G.E., Olivero, J.J., Evans, W.F.J., Debrestian, D.J., Chardon, L., 2002. Three-satellite comparison of polar mesospheric clouds: Evidence for long-term change. Journal of Geophysical Research, 107(D12), 4134, doi:10.1029/2001JD000668.
8. Thomas G. E., Olivero, J.J., DeLand, M., Shettle, E.P., Comment on "Are noctilucent clouds truly a 'miner's canary' for global change?". *EOS, 84(36)*, 2003.
9. von Zahn, U., Are noctilucent clouds truly a "miner's canary" for global change?. *EOS, 84(28)*, 2003.
10. Russell, J. M. III, L. L. Gordley, J. H. Park, S. R. Drayson, W. D. Hesketh, R. J. Cicerone, A. F. Tuck, J. E. Frederick, J. E. Harries, and P. J. Crutzen, The Halogen Occultation Experiment, *J. Geophys. Res*., *98*, 10,777-10,797, 1993.
11. Gordley, L. L., B. T. Marshall, and D. A. Chu, LINEPAK: Algorithms for modeling spectral transmittance and Radiance, *JQSRT, 52*, p563, 1994.